A New MnO_x Cathode Material for Rechargeable Lithium Batteries

Arno Perner,*[a] K. Holl,[a] D. Ilic,[a] and M. Wohlfahrt-Mehrens[b]

Keywords: Lithium batteries / Manganese oxides / Cathode materials

Different manganese oxide phases have been synthesized. Rietveld analysis of XRD profiles and galvanostatic cycling in 2025 coin cells were performed for structural and electrochemical characterization. A new two-phase product, containing α-MnO_2 and β-MnO_2 components, was found to deliver better electrochemical results than single phase α-MnO_2, β-MnO_2 or α/ramsdellite-MnO_2. It is shown that the β-MnO_2 phase is responsible for the high discharge capacities and that the α-MnO_2 is responsible for a stable structure during lithium intercalation and extraction, as the hollandite structure shows a small unit-cell volume change. This new cathode material is therefore a β-MnO_2 phase stabilized with α-MnO_2. Furthermore, the reaction of the new α/β-MnO_2 with LiOH was examined. Some lithium atoms of LiOH are intercalated within the channels as Li_2O in order to stabilize the structure, so that no capacity loss after the first cycle appears, whilst others form a $Li_2O{\cdot}MnO_2$ phase that delivers an additional structure stabilization and therefore a better cycling performance.

Introduction

The development of secondary lithium batteries involves the use of high performance cathodic materials with numerous requirements such as high gravimetric and volume capacity, high density, high standard potential, fast electrode kinetics, reversible insertion reaction, satisfactory electronic conductivity, low solubility, a relatively low price for production, low toxicity, chemical compatibility with the electrolyte and good rechargeability. Therefore, intensive research has been carried out in the field of rechargeable positive electrodes.[1−9]

Manganese oxides are of interest as insertion electrodes for both primary and secondary lithium batteries.[10] The rechargeability of 3 V manganese oxide electrodes tends to be limited by the anisotropic expansion and contraction of the crystallographic unit cell when lithium is inserted into, and removed from, the manganese oxide. 3 V positive materials are used, for example, in button cells of different sizes for memory back-up (MBU) and bridging applications.[11]

The goal of this paper was to optimize 3 V cathode materials in order to improve the cycling stability and the discharge capacities. To fulfill these requirements we focused our efforts on stabilizing the α-MnO_2 structure with foreign phases. The structure of α-MnO_2 with the large [2 × 2] channels of the hollandite framework is not stable to lithium insertion/extraction. These [2 × 2] tunnels are usually occupied by cations (e.g. Ba^{2+}, K^+...) or water molecules (as OH^-) which hinder the lithium ion diffusion within the channels. As a consequence the α-MnO_2 framework must be stabilized by replacing these cations or water molecules with Li_2O[12,13] or by adding foreign phases[14] (e.g. ramsdellite-MnO_2, pyrolusite).

Thackeray proposed an α-MnO_2 (hollandite) structure stabilized with ramsdellite-MnO_2, which delivers higher discharge capacities than single-phase α-MnO_2 or ramsdellite-MnO_2.[14]

We report here a transformation of α/ramsdellite-MnO_2 when annealing at 350 °C. As a thermal transformation of ramsdellite to β-MnO_2 (pyrolusite) was observed by Ramsdell,[15] we assume a transformation of α/ramsdellite-MnO_2 to α/β-MnO_2. The structure and electrochemical properties of single-phase α-MnO_2, ramsdellite-MnO_2, β-MnO_2, α /ramsdellite-MnO_2 and the new α/β-MnO_2 are compared.

All these manganese oxides suffer from a large irreversible capacity loss after the first discharge (up to 30%) due to lithium trapped within the channels in order to stabilize the structure. The manganese oxides are chemically lithiated to reduce this irreversible capacity loss. We also observe that a reaction of the MnO_2 samples with LiOH results in a product consisting of lithium-stabilized MnO_2 with lithium intercalated within the channels [16] and an $Li_2O{\cdot}MnO_2$ phase.

[a] VARTA Gerätebatterie GmbH
Daimlerstrasse 1, 73479 Ellwangen, Germany
Fax: (internat.) + 49-(0)7961/83511
E-mail: arno.perner@varta.com
[b] Centre for Solar Energy and Hydrogen Research Baden-Wuerttemberg,
Helmholtzstr.8, 89081 Ulm, Germany

Results and Discussion

Structure

The new α/β-MnO_2 was synthesized by annealing α/ramsdellite-MnO_2 at 350 °C for several hours. Figure 1 shows the TG/DSC graph of α/ramsdellite-MnO_2 with endothermic peaks at 100−150 °C and 170−220 °C due to the loss of surface adsorbed water and structural water, respectively. There is an additional endothermic peak at around 300 °C due to the transformation of α/ramsdellite-MnO_2 to α/β-MnO_2.

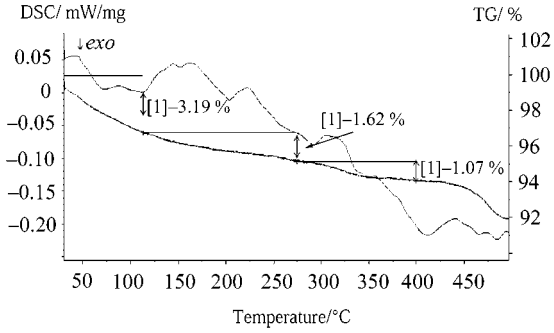

Figure 1. TG/DSC graph of α/Ramsdellite-MnO_2 with an endothermic peak at about 300 °C due to the transformation of α/Ramsdellite-MnO_2 to α/β-MnO_2

Figure 2 shows the different XRD patterns of single-phase α-MnO_2 with the hollandite structure, α/ramsdellite-MnO_2 [14] with the characteristic ramsdellite-MnO_2 Bragg line [110] at 22° and the new α/β-MnO_2. The pattern is characteristic of a two-phase product consisting of α-MnO_2 with a tetragonal unit cell (space group *I*4/*m*) and a β-MnO_2 phase with a pyrolusite structure (tetragonal symmetry).

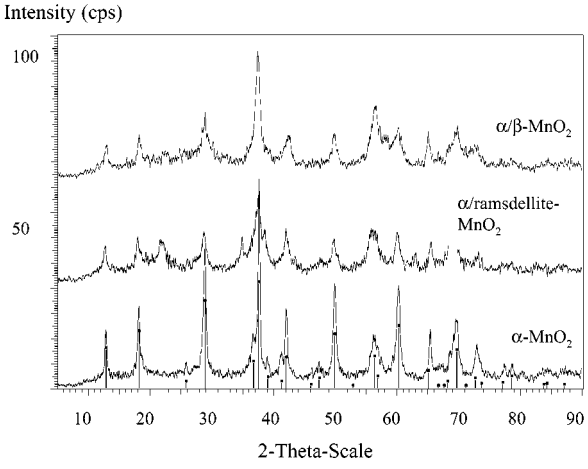

Figure 2. The different XRD patterns of single-phase α-MnO_2 with the hollandite structure, α/ramsdellite-MnO_2 with the characteristic Ramsdellite-MnO_2 reflex [110] at 22° and the new α/β-MnO_2

Table 1 compiles some characteristic reflexes of α-MnO_2 and β-MnO_2. The XRD lines at about 2θ = 28, 37, 42 and 56° of single phase α-MnO_2 coincide with the XRD lines of β-MnO_2. Figure 3 demonstrates that the [141], [600] and [521] lines recorded for α-MnO_2 are similar to the α/β-MnO_2 pattern, although there is an obvious difference in peak intensities. The XRD peak at about 56° of the synthesized α/β-MnO_2 shows a higher intensity than that of the single phase α-MnO_2 peak as the [211] line of β-MnO_2 coincides with the α-MnO_2 [600] line.

Table 1. Characteristic reflexes of α-MnO_2 and β-MnO_2

2θ (°)	Phase	*hkl*
12.781	α-MnO_2	[110]
18.112	α-MnO_2	[200]
28.882	α-MnO_2	[310]
28.670	β-MnO_2	[110]
37.488	α-MnO_2	[211]
37.342	β-MnO_2	[101]
41.993	α-MnO_2	[301]
42.800	β-MnO_2	[111]
49.847	α-MnO_2	[141]
56.356	α-MnO_2	[600]
56.645	β-MnO_2	[211]
60.253	α-MnO_2	[521]
59.363	β-MnO_2	[220]

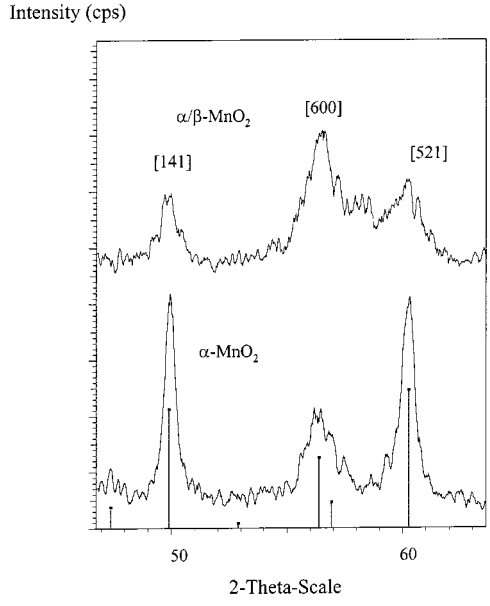

Figure 3. The [141], [600] and [521] reflexes of the measured XRD pattern of α-MnO_2 compared with the α/β-MnO_2 pattern

A [001] projection of the α-MnO_2 framework structure is given in Figure 4. The structure consists of [2×2] tunnels and of [1×1] tunnels with the pyrolusite structure. The structure of α/β-MnO_2 can be described by the model shown in Figure 5. It has an intergrown structure of layers of [2×2] channels and layers of [1×1] channels with disordered stacking. Layers with the hollandite structure alternate with several layers with the pyrolusite structure.

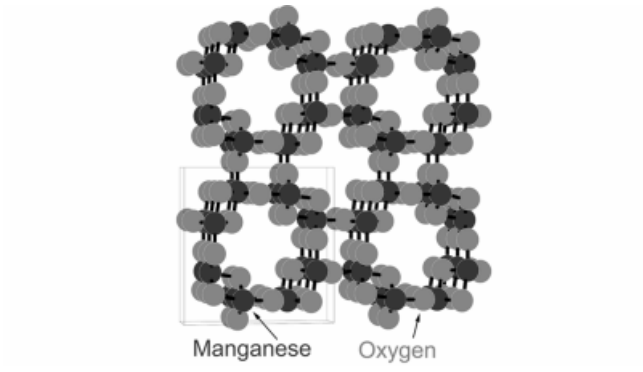

Figure 4. [001] projection of the α-MnO_2 framework structure

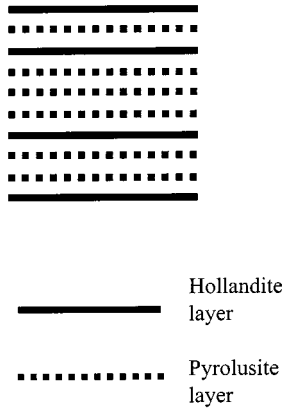

Figure 5. Proposed model of the α/β-MnO_2 structure

Figure 6 shows the Rietveld analysis (GOF: 1.35; *R*: 8.71) of the observed and calculated XRD pattern of α/β-MnO_2, assuming this structural model (α-MnO_2: PDF data 44−141; β-MnO_2: PDF data 24−735). There is quite a good agreement between the calculated pattern and the observed one. The cell parameters of a supposed tetragonal unit cell are: a = 9.791 Å and c = 2.862 Å. A peak can be observed at about 22° that doesn't belong either to the α-MnO_2 phase or to the β-MnO_2 phase. This peak can be assigned to ramsdellite-MnO_2 that has not completely transformed to β-MnO_2. As a consequence this new MnO_2 sample is a three-phase product consisting of α-MnO_2, β-MnO_2 and ramsdellite-MnO_2. The phase analysis yielded a composition of 56% α-MnO_2, 41% β-MnO_2 and 4% ramsdellite-MnO_2.

Electrochemistry

Figure 7 and 8 show the first discharge curves and the cycling behaviour, respectively, of single-phase α-MnO_2, β-MnO_2, ramsdellite-MnO_2 and the two-phase samples α/ramsdellite-MnO_2 and α/β-MnO_2. It is obvious that the stabilized α-MnO_2 delivers higher discharge capacities than single-phase α-MnO_2. Furthermore, β-MnO_2 and ramsdellite-MnO_2 show the highest discharge capacities. Single-phase α-MnO_2 shows an s-shaped discharge curve whereas β-MnO_2, ramsdellite-MnO_2 and the stabilized α-MnO_2 ex-

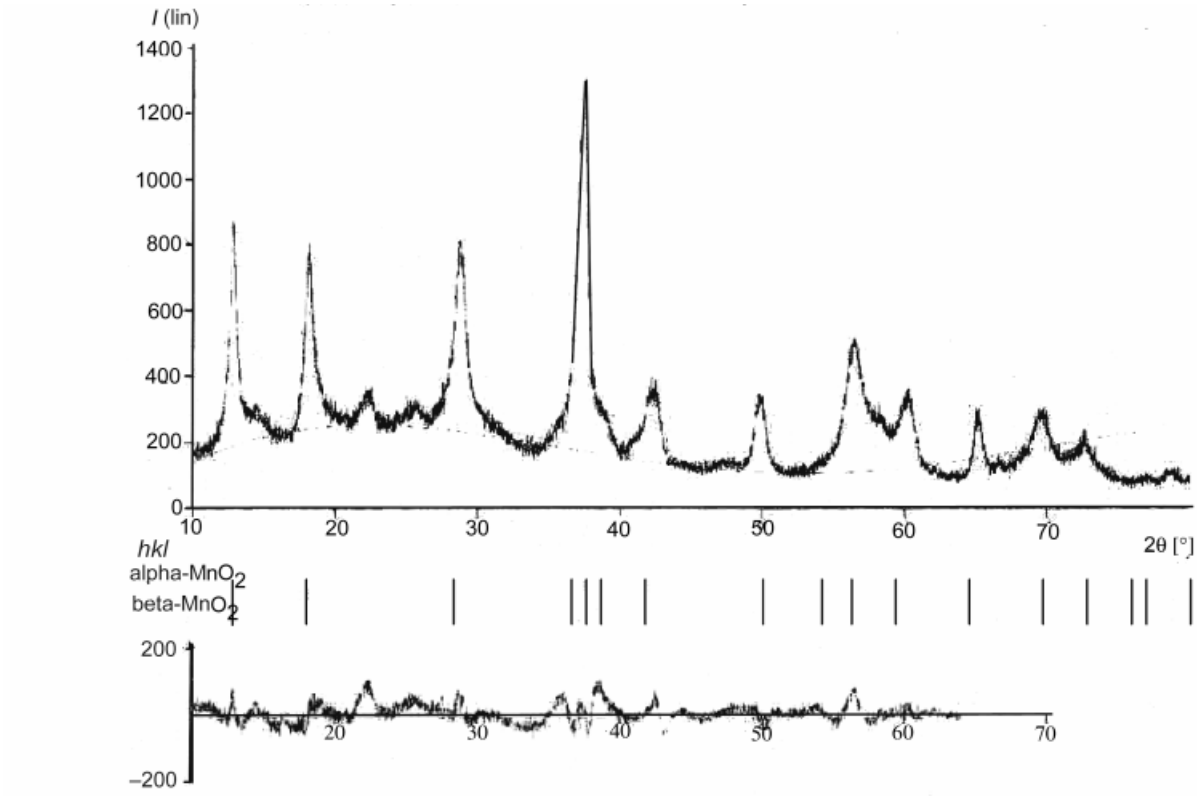

Figure 6. Observed and calculated (by Rietveld-method) XRD pattern of α/β-MnO_2 and the difference between these two patterns

hibit flat discharge curves with two voltage plateaux. The best cycling behaviour is obtained for single-phase α-MnO_2, due to small changes to the lattice parameters and unit cell volume,[18] single-phase ramsdellite-MnO_2 and the new α/β-MnO_2. The good cycling behaviour of ramsdellite-MnO_2 can be explained by a very small volume expansion and contraction during cycling, in contrast to other reports.[17] β-MnO_2 provides quite a good cycling performance even though it has always described as a cathode material for primary batteries.[19] Further work is underway to understand this feature in detail.

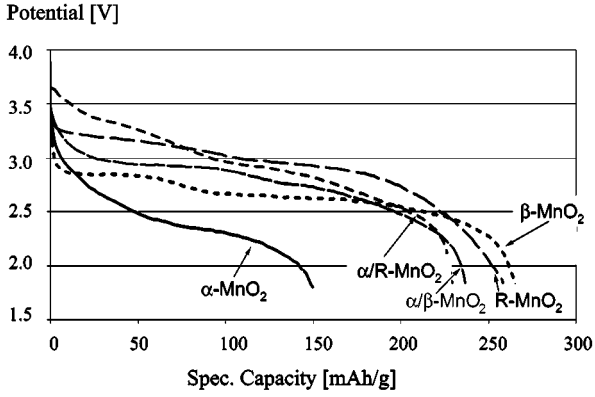

Figure 7. First discharge curves of single-phase α-MnO_2, β-MnO_2, ramsdellite-MnO_2 and the two-phase samples α/ramsdellite-MnO_2 and α/β-MnO_2

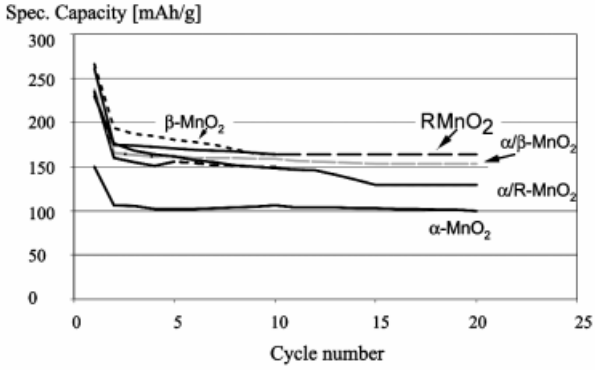

Figure 8. Cycling behaviour of single-phase α-MnO_2, β-MnO_2, ramsdellite-MnO_2 and the two-phase samples α/ramsdellite-MnO_2 and α/β-MnO_2

On the initial discharge the new α/β-MnO_2 electrode achieves a specific capacity of 237 mAh/g. After a decrease of the capacity to 168 mAh/g on the second discharge, the electrode shows good rechargeability, yielding 160 mAh/g after 10 cycles. The initial capacity loss of 30% suggests that about 0.3 mol of inserted lithium is used to provide the MnO_2 electrode with enhanced structural stability, and that this stabilizing lithium cannot easily be removed from the structure. Figure 9 shows the differential capacity plot of α/β-MnO_2 for the first and second cycle. The sharp intercalation peak at 2.9 V decreases in the second discharge due to partially irreversible intercalated lithium ions that stabilize the electrode structure during cycling. The extraction of the reversible ions from the [2×2] and [1×1] tunnel structure takes place at between 3.0 and 3.2 V, which is a higher deintercalation potential than the intercalation potential. This potential difference is mainly due to the slow kinetics of the lithium ions during extraction from the channels. The two voltage plateaux in the discharge profile of the two-phase α/β-MnO_2 are explained by the different intercalation sites.

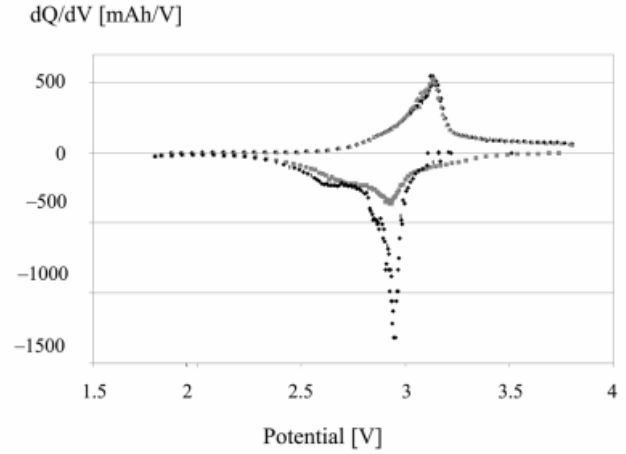

Figure 9. Differential capacity plot of α/β-MnO_2 (first and second cycle)

The high discharge capacities and the good cycling behaviour after the first cycle of this new two-phase product can be explained by the existence of interconnected α-MnO_2 and β-MnO_2 phase in the electrode structure. The β-MnO_2 is responsible for the high discharge capacities and flat discharge curve, whereas the α-MnO_2 is responsible for a stable structure during lithium intercalation and extraction, as the hollandite structure shows a small unit cell volume change. This new cathode material is therefore a β-MnO_2 stabilized with α-MnO_2.

Lithiated Manganese Oxides

In order to reduce the irreversible capacity loss after the first discharge the samples were lithiated with LiOH. Ohzuku et al. proposed a lithiation of EMD or heat-treated EMD with LiOH or other lithium salts.[21−23] This electrode material is a composite of γ-MnO_2 and β-MnO_2. Thackeray et al. described a lithiation of single-phase α-MnO_2 with LiOH.[18]

Figure 10 gives the XRD patterns of different lithiated α-MnO_2 samples. These patterns show two-phase products consisting of α-MnO_2 and a $Li_2O{\cdot}MnO_2$ (Li_2MnO_3) phase with the rock-salt structure ([002] peak at 18.7°). A different amount of $Li_2O{\cdot}MnO_2$ can be observed depending on the temperature and duration of the reaction with LiOH. There is only a small capacity loss of 5% observable after the first intercalation. The electrode structure is stabilized by Li_2O molecules introduced into the channels.[16] It appears that

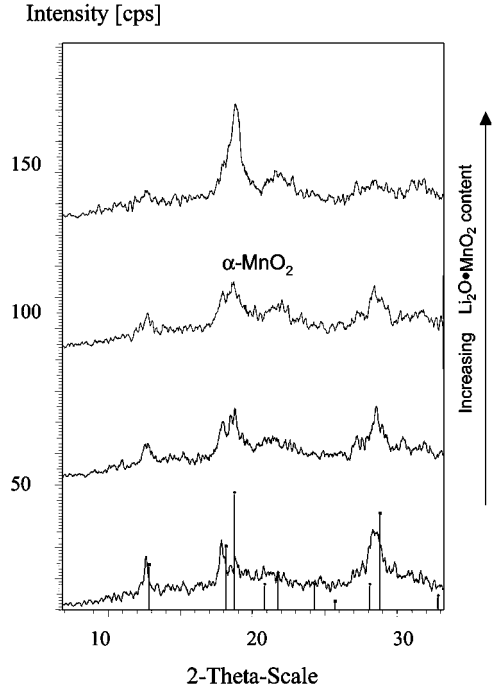

Figure 10. XRD patterns of α-MnO_2 with different Li_2MnO_3 content

no more lithium ions are trapped within the tunnels in order to stabilize the structure during electrochemical cycling. Our experiments proved that about 30% of the intercalation sites are necessary to stabilize the electrode structure. This stabilization can be done either electrochemically with lithium ions or chemically with Li_2O molecules (reaction with LiOH). It is therefore possible to insert/extract 0.7 mol of lithium reversibly.

The $Li_2O{\cdot}MnO_2$ phase provides an additional stabilization of the electrode that is responsible for a better cycling performance. The correlation between the amount of $Li_2O{\cdot}MnO_2$ and the cycling behaviour is shown in Figure 11. The capacity loss per cycle and the molar quantity of rechargeable lithium are plotted against the $Li_2O{\cdot}MnO_2$ content. The $Li_2O{\cdot}MnO_2$ phase stabilizes as a matrix (i.e. a stable rock salt structure) the large [2×2] channel structure of the α-MnO_2 framework. With increasing $Li_2O{\cdot}MnO_2$

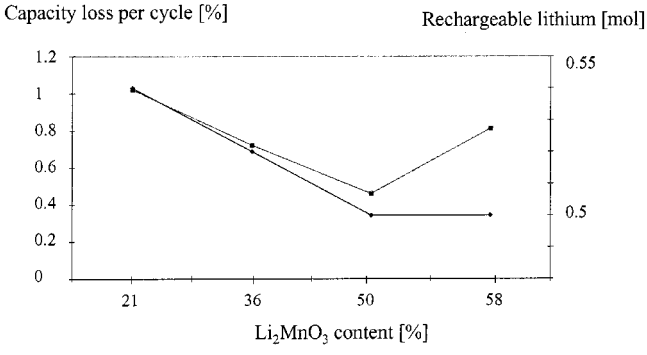

Figure 11. Correlation between Li_2MnO_3 content and cycling behaviour

content the rechargeable lithium decreases as $Li_2O{\cdot}MnO_2$ delivers only low discharge capacities.[20] We obtained the best electrochemical performance with about 30−40% $Li_2O{\cdot}MnO_2$.

The first discharge curves and the cycling behaviour of the lithiated α/β-MnO_2 in comparison to the other MnO_2 phases are shown in Figure 12 and 13, respectively. This lithiated α/β-MnO_2 is a MnO_2-based composite of α-MnO_2 and β-MnO_2 with Li_2MnO_3 as an additional phase. All the lithiated electrode materials show no, or only a small, capacity loss after the first cycle. The best electrochemical results were obtained with the lithiated α/β-MnO_2, which delivers a flat discharge curve and a good cycling stability with high discharge capacities (190 mAh/g after 10 cycles).

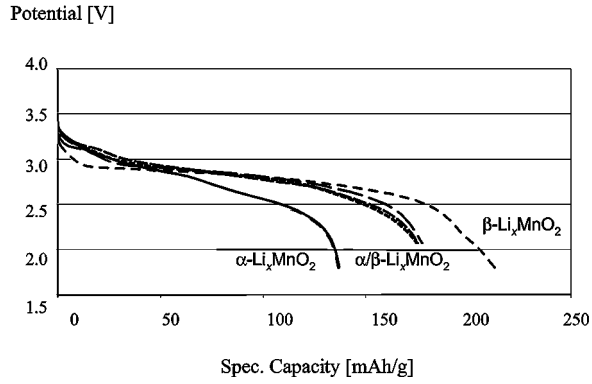

Figure 12. First discharge curves of lithiated manganese oxide phases

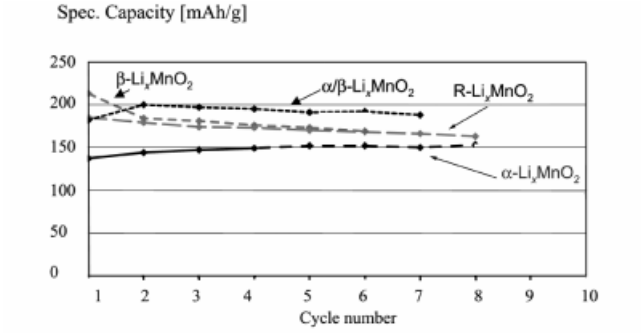

Figure 13. Cycling behaviour of the lithiated manganese oxide phases

The differential capacity plot of lithiated α/β-MnO_2 is displayed in Figure 14. There is no difference in peak intensities between the first and second cycles and there are two additional reduction/oxidation peaks in comparison to the non-lithiated α/β-MnO_2 phase. The peaks at 3.5 and 2.8 V are due to the presence of other lithium intercalation sites in the $Li_2O{\cdot}MnO_2$ framework.

Conclusion

We have demonstrated that a new synthesized α/β-MnO_2 electrode, containing α-MnO_2 and β-MnO_2 components,

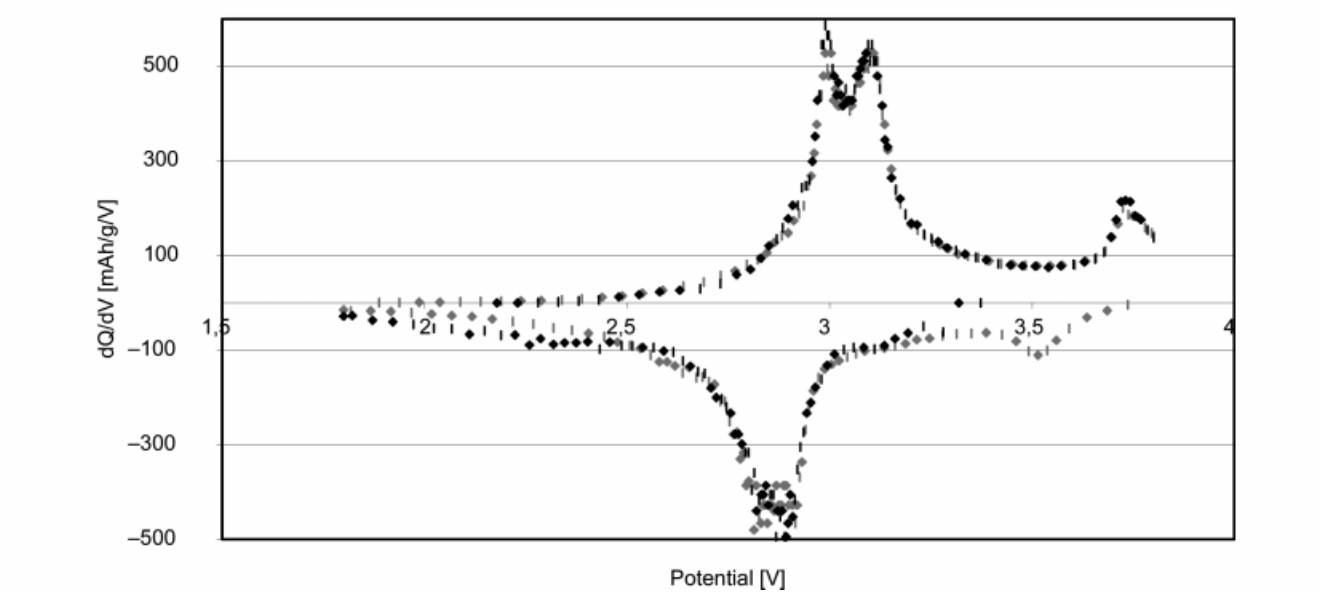

Figure 14. Differential capacity plot of lithiated α/β-MnO_2

exhibits better electrochemical features than either single phase α-MnO_2, β-MnO_2 or α/ramsdellite-MnO_2. Furthermore, it has been shown that a reaction of α-MnO_2 with LiOH forms a two-phase product consisting of a mixture of α-MnO_2 and a $Li_2O{\cdot}MnO_2$ phase. Some lithium ions of the LiOH are intercalated within the channels as Li_2O in order to stabilize the structure.[16] No capacity loss appears after the first cycle, and some lithium ions form a $Li_2O{\cdot}MnO_2$ phase that delivers an additional structure stabilization and therefore a better cycling performance. The electrochemical data indicate that lithiated α/β-MnO_2, which is a composite electrode of α-MnO_2, β-MnO_2 and Li_2MnO_3 as an additional phase, is an attractive 3 V electrode material that provides a betterr electrochemical performance than single-phase manganese oxides, with discharge capacities of 190 mAh/g after several cycles.

Experimental Section

Synthesis: The different α-MnO_2 samples were synthesized by treating α-Mn_2O_3 with sulfuric acid at different temperatures for several days with constant stirring. α-Mn_2O_3 (bixbyite-type structure) was obtained by heating EMD (Mitsui TAD 2) in air at 700 °C for 16 hours. Ramsdellite-MnO_2 was synthesized by treating a $LiMn_2O_4$ spinel with sulfuric acid. This ramsdellite-MnO_2 transforms to β-MnO_2 when heated to 350 °C for several hours. Lithiated samples were obtained by heat treatment of the different MnO_2 with LiOH between 300 and 400 °C for several hours.

Structural Characterization: X-ray diffraction profiles of the samples were determined with a Siemens D5000 diffractometer (Cu-K_α radiation). Scans were measured in the range from $2\theta = 5°$ up to 90° with a step size of 0.02°. Phase analysis was performed using the Bruker AXS software package Diffrac AT. Structural parameters were determined by Rietveld analysis of the diffraction profiles using the Bruker AXS program Win-Rietveld.

Electrochemical Characterization: Each electrode sample was prepared by grinding and mixing the active material with 4 wt.% carbon (Ketjenblack EC600) and 6 wt.% PTFE pressed into a tablet (diam 20 mm) under a pressure of 2 t/cm^2. The electrodes were dried for 16 h in vacuo at 120 °C. The separator was a polypropylene sheet (Celgard). The galvanostatic cycling took place in 2025 coin cells against metallic Li. As electrolyte a 1 M solution of $LiPF_6$ in ethylene carbonate (EC):ethylmethyl carbonate (EMC) (1:1) was used (Merck LP50). The cells were cycled galvanostatically between 3.8 and 1.8 V at a current density of 0.5 mA/cm^2 on a MACCOR test equipment. Cell assembly was performed in a glove box under argon atmosphere at room temperature.

TG/DSC measurements: The TG/DSC measurements were performed on a thermogravimetric analyser (TGA, Netsch STA 409, 5 K/min).

[1] A. Eichinger, J. O. Besenhard, *J. Electroanal. Chem.* **1976**, *72*, 1.
[2] M. S. Whittingham, *Science* **1976**, *192*, 1126.
[3] G. L. Holleck, J. P. Driscoll, *Electrochim. Acta* **1977**, *22*, 647.
[4] M. S. Whittingham, *Prog. Solid. State Chem.* **1978**, *12*, 41.
[5] D. W. Murphy, P. A. Christian, *Science* **1979**, *205*, 651.
[6] K. M. Abraham, *J. Power Sources* **1982**, *7*, 1.
[7] G. Pistoia, *J. Power Sources* **1983**, *9*, 307.
[8] J. P. Gabano, *Lithium Batteries*, Academic Press Ltd London, **1983**.
[9] J. Desilvestro, O. Haas, *J. Electrochem. Soc.* **1990**, *137*, 5C.
[10] M. M. Thackeray, M. H. Rossouw, A. de Kock, A. P. de la Harpe, R. J. Gummow, K. Pearce, D. C. Liles, *J. Power Sources* **1993**, *43−44*, 289−300.
[11] D. Ilic, M. Kilb, K. Holl, H. W. Praas, E. Pytlik, *J. Power Sources* **1999**, *80*, 112−115.
[12] C. S. Johnson, D. W. Dees, M. F. Mansuetto, M. M. Thackeray, D. R. Vissars, D. Argyriou, C.-K. Loong, L. Christensen, *J. Power Sources* **1997**, *68*, 570−577.

[13] M. A. Humbert, Ph. Biensan, M. Broussely, A. Lecref, A. Dolle′, H. Ladhily, *J. Power Sources* **1993**, *43−44*, 681−687.

[14] C. S. Johnson, M. F. Mansuetto, M. M. Thackeray, Y. Shao Horn, S. H. Hackney, *J. Electrochem. Soc.* **1997**, *144*, 2279−2283.

[15] L. S. Ramsdell, *Am. Mineral.* **1932**, *17*, 143−149.

[16] C. S. Johnson, D. W. Dees, M. F. Mansuetto, M. M. Thackeray, D. R. Vissers, D. Argyriou, C. K. Loong, L. Christensen, Abstract 874, p.1076, *The Electrochemical Society Meeting Abstracts*, Vol. 96−2, San Antonio, TX, Oct. 6−11, **1996**.

[17] M. M. Thackeray, M. H. Rossouw, R. J. Gummow, D. C. Liles, K. Pearce, A. de Kock, W. I. F. David, S. Hull, *Electrochim. Acta* **1993**, *38*, 1259.

[18] M. H. Rossouw, D. C. Liles, M. M. Thackeray, W. I. F. David, S. Hull, *Mat. Res. Bull.* **1992**, *27*, 221−230.

[19] M. M. Thackeray, *Prog. Batteries Battery Mater.* **1995**, *14*, 1−87.

[20] P. Kalyani, S. Chitra, T. Mohan, S. Gopukumar, *J. Power Sources* **1999**, *80*, 103−106.

[21] T. Ohzuku, K. Sawai, T. Hirai, *Chem. Express* **1989**, *4*, 777−780.

[22] T. Ohzuku, K. Sawai, T. Hirai, *Chem. Express* **1989**, *4*, 773−776.

[23] T. Ohzuku, K. Sawai, T. Hirai, *Proc. Electrochem. Soc.* **1991**, *91*, 318−325.

Received June 25, 2001
[I01226]